Image-domain least-squares reverse-time migration through point spread functions

Jianyong Bai and Orhan Yilmaz, Emerson*

SUMMARY

Imaging technologies, such as reverse-time migration (RTM), generate migration images for complex structures. However, the migrations can be distorted due to undersampled acquisition geometry, limited recording aperture and illumination effects. In order to partially correct the distortions, we present multi-iteration image-domain least-squares migration (LSM) by approximating the Hessian through point spread functions (PSFs). Since information in a migration image is insufficient to uniquely determine a reasonable reflectivity model and LSM itself can cause artifacts, we include an L_p-norm regularization of the difference between the migration image and the reflectivity model and a total variation (TV) regularization of the reflectivity model. The L_p-norm regularization reduces artifacts and makes the reflectivity model to be similar to the migration image, while the TV regularization helps to maintain structural continuity. We illustrate the LSM through RTM. Given a migration velocity model, synthetic data for a grid of scatterer points is generated through Born modeling operators and, then, is migrated to calculate PSFs. A reflectivity model is convolved with the PSFs to match a migration image. We use a nonlinear conjugate gradient method to seek an optimal reflectivity model. Preliminary results from numerical examples show that the scheme is helpful to improve resolution and reduce artifacts in image domain and broadens spectrum in wavenumber domain.

INTRODUCTION

Seismic data can be viewed as the result of forward modeling process through subsurface structures, while seismic migration reverses the forward process, thereby re-locating seismic events to the locations where the events occur in the subsurface and generating an accurate image of the subsurface. The state-of-the-art imaging technologies for complex structures, such as Kirchhoff migration (Claerbout, 1985), one-way wave-equation method (Ristow and Rühl, 1997), and RTM (Baysal et al., 1992), are widely applied to generate seismic images in the petroleum industry. However, seismic migration can be distorted by undersampled acquisition geometry, limited recording aperture, wavelet stretch, various noise such as ocean waves and anthropogenic noise, illumination effects in the complex structures, and inaccurate wave propagators such as in the case of anisotropic or viscoelastic cases.

In order to partially overcome the above-mentioned effects of the distortions, single- or multi-iteration least-squares migration (LSM) has been proposed. Benefits of LSM include improved image quality in both seismic event continuity and resolution, better illumination, deghosting, more balanced amplitudes, and reductions in migration artifacts and noise. Data-domain LSM generates synthetic data from a reflectivity model and finds an optimal model so that the synthetic data obtained from the model fits field seismic data (Nemeth et al., 1999). It is well known that the multi-iteration data-domain LSM, especially least-squares RTM, can be computationally prohibitive for 3D marine streamer data. In contrast, image-domain LSM creates an image through a Hessian matrix, an operator of demigration followed by migration, from a reflectivity model. An optimal model is obtained so that the image generated from the model fits the raw migrated image (Aoki and Schuster, 2009). Since the storage and computation of the Hessian and its inverse is expensive, alternative methods have been developed to approximate the Hessian and its inverse. Guitton (2004) used non-stationary matching filters to approximate the inverse of the Hessian while Fletcher et al. (2012) used point spread functions (PSFs) to approximate the Hessian. In order to obtain an unique solution and reduce artifacts in a reflectivity model due to incomplete surface data and irregular subsurface illumination, LSM with various constraints have also been developed. Wu et al. (2016) presented a data-domain least-squares RTM with an L_1-norm of the reflectivity model. Fletcher et al. (2012) included an L_p-norm of reflectivity and an L_2-norm of model change. Guo and Wang (2020) introduced both a sparse regularization for reflectivity constraint and a total-variation (TV) regularization for structural continuity in image-domain LSM by non-stationary matching filters.

In this paper we propose multi-iteration image-domain LSM by approximating the Hessian through PSFs with L_p-norm regularization of the difference between a migration image and a reflectivity model, and a TV regularization of the reflectivity model. The L_p-norm regularization is introduced to reduce artifacts, while the TV regularization is added to keep structural continuity. Based on the LSM scheme, we implement multi-iteration image-domain least-squares RTM. Given a migration velocity model, synthetic seismic data for a grid of scatterer points is generated from Born modeling operators and, then, is migrated through RTM to calculate PSFs. A reflectivity model is convolved with the PSFs to match a migration image. An optimal reflectivity model is obtained through a nonlinear conjugate gradient method. We test the LSM scheme for the L_2- and L_1-norm regularizations of the difference between a migration image and a reflectivity model. Preliminary results from numerical examples demonstrate that the scheme improves resolution and reduces artifacts in the image domain, and thus broadens amplitude spectrum in wavenumber (k_x - k_z) domain.

THEORY

Given a reflectivity model $\mathbf{m}$, seismic data $\mathbf{d}$ is calculated through a forward modeling operator $\mathbf{L}$

$$\mathbf{d} = \mathbf{L}\mathbf{m}. \tag{1}$$

The forward modeling operator $\mathbf{L}$ is associated with acquisition geometry, source wavelet and physical parameter models.

Migration image $\mathbf{m}_{mig}$ is obtained through a migration operator, the adjoint of the forward modeling operator $\mathbf{L}$,

$$\mathbf{m}_{mig} = \mathbf{L}^T\mathbf{d}. \tag{2}$$

Equations 1 and 2 lead to the relationship between the migration image and the reflectivity model

$$\mathbf{m}_{mig} = \mathbf{H}\mathbf{m}, \tag{3}$$

where $\mathbf{H} = \mathbf{L}^T\mathbf{L}$ denotes the Hessian matrix. Equation 3 states that the migration image $\mathbf{m}_{mig}$ is the blurred version of the reflectivity model $\mathbf{m}$ by the Hessian matrix $\mathbf{H}$. In general, the Hessian is a function of velocities and acquisition geometry. It is a measurement of resolution and illumination, and determines the degree of blurring that a point in $\mathbf{m}$ exhibits in $\mathbf{m}_{mig}$.

According to Equation 3, we set up a nonlinear image deblurring problem, which minimizes the following objective function in order to eliminate the blurring effects caused by the Hessian,

$$J(\mathbf{m}) = \frac{1}{2}||\mathbf{H}\mathbf{m}-\mathbf{m}_{mig}||_2^2 + \alpha||\mathbf{m}-\mathbf{m}_{mig}||_p + \beta\int_\Omega ||\nabla\mathbf{m}||_1 d\mathbf{x}, \tag{4}$$

where $||\cdot||_2$, $||\cdot||_p$, and $||\cdot||_1$ represent L_2-, L_p-, and L_1-norm, respectively, $\nabla\mathbf{m}$ is the gradient of $\mathbf{m}$ with respect to the coordinates $\mathbf{x}$ in the spatial space Ω, α and β are the weights for the 2nd and 3rd terms, respectively. It is well known that there is insufficient information in $\mathbf{m}_{mig}$ to uniquely determine a plausible reflectivity model, making deblurring an ill-posed problem. In addition, $\mathbf{m}_{mig}$ contains various noises which complicate the task of determining the reflectivity model $\mathbf{m}$. Such problems are generally solved by the use of regularizations to mitigate the ill-posedness of the problem and obtain reasonable results. In Equation 4, the 2nd term is helpful to reduce the artifacts in $\mathbf{m}$ and make sure that $\mathbf{m}$ is always similar to $\mathbf{m}_{mig}$, while the 3rd term is the total variation (TV) regularization which can maintain the continuity of geological structures in $\mathbf{m}$. The parameters α and β can be determined according to variances (Bai and Yingst, 2014) or generalized cross-validation (Golub and von Matt, 1997). Since the objective function J contains the TV term, we choose a nonlinear conjugate gradient method when solving for the optimal model $\mathbf{m}$ to minimize J.

Since the size of $\mathbf{H}$ is large, the computation and storage of $\mathbf{H}$ is expensive for real problems. Therefore, approximations of the Hessian are usually used. In this method the Hessian is approximated by PSFs (Lecomte, 2008; Fletcher et al., 2012). We generate the synthetic seismic data of a grid of scatterer points through linearized Born forward modeling operators. First the wavefields $P_0(\mathbf{x},t)$ is extrapolated forward in time

$$\frac{1}{V^2}\frac{\partial^2 P_0}{\partial t^2} = \nabla P_0 + f(\mathbf{x}_s,t), \tag{5}$$

where $V = V(\mathbf{x})$ is the migration velocity at the position $\mathbf{x}$, and $f(\mathbf{x}_s,t)$ is the source wavelet at the source position $\mathbf{x}_s$ and at time t. Second, we propagate the wavefields $P(\mathbf{x},t)$ backward in time and, at the same time, inject a reflectivity model r at each position $\mathbf{x}$

$$\frac{1}{V^2}\frac{\partial^2 P}{\partial t^2} = \nabla P + \frac{2r}{V^2}\frac{\partial^2 P_0}{\partial t^2}. \tag{6}$$

In the method, the grid of scatterer points is used as $r(\mathbf{x})$ and $P(\mathbf{x},t)$ is used for the generation of synthetic data at receiver positions. Finally, the synthetic data is migrated through RTM to get impulse responses, i.e. the PSFs which represent the Hessian, at each scatterer point. The Hessian at other imaging points is obtained by interpolation from surrounding computed PSFs.

EXAMPLES

We test the proposed LSM scheme on a modified Marmousi model which contains a water body from surface down to 500 meters. The velocity model is displayed in Figure 1(a), while its smoothed version is shown in Figure 1(b). The modeling operator $\mathbf{L}$ and the migration operator $\mathbf{L}^T$ are based on two-way wave-equation solved by a 4th-order finite-difference (FD) method with a convolutional perfectly-matched layer absorbing boundary condition in the time-space domain.

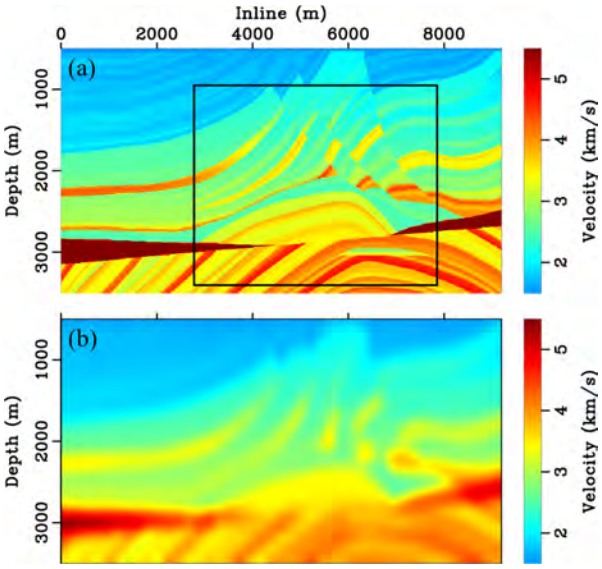

Figure 1: (a) Velocity model. (b) Smoothed velocity model obtained by using a smoothing length of 200 meters in both directions. Water body (from surface down to 500 m) is not shown. The velocity in water is 1.5 km/s.

We approximate the Hessian by Born modeling followed by RTM to a grid of point scatters in the velocity space under water. The smoothed velocity model shown in Figure 1(b) is used for this purpose. In order to capture significant variations in illumination and blurring effects and, at the same time, avoid the adjacent PSFs overlapping, the interval of scatterer points is chosen to be 400 meters in both directions. The Born modeling synthetic data is generated with a record length of 4 seconds. The synthetic data includes 115 shots with a shot interval of 80 meters. Each shot gather has 921 receivers with a receiver interval of 10 meters. A Ricker wavelet with the peak frequency of 15 Hz is used. The synthetic data is migrated to get the impulse responses for each scatterer point, which are

known as PSFs. Figure 2 shows the migration of the regular grid of scatterer points. The image is from the highlighted rectangular area in Figure 1(a). Significant variations are observed in both directions among the computed PSFs. For a location where we do not compute a PSF, we calculate its PSF through the bi-linear interpolation of its surrounding PSFs.

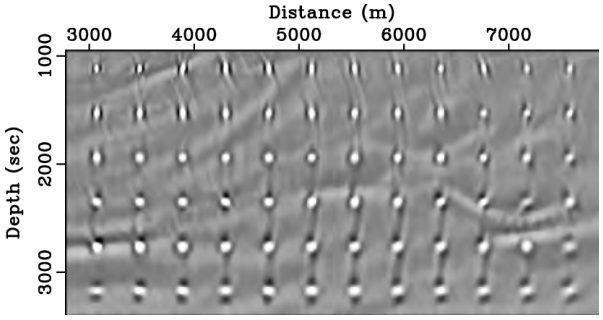

Figure 2: PSFs in the rectangular area highlighted in Figure 1(a). The PSFs are calculated from the smoothed model in Figure 1(b).

For the purpose of verifying that the proposed method can give a good approximation of the Hessian and can eliminate the blurring effects caused by the Hessian, reflectivities are calculated from the velocity model shown in Figure 1(a). The reflectivities are displayed in Figure 3(a). We convolve the reflectivities with the calculated PSFs in Figure 2 to obtain an image as shown in Figure 3(b). According to Equation 3, the image is approximately equal to a conventional migration image $\mathbf{m}_{mig}$ since the PSFs approximate the Hessian matrix and actually act as a blurring operator. As a result, the resolution of Figure 3(b) is much lower than the one of Figure 3(a). The blurring effects soften the edges of reflectivities and hide some geological structures for seismic interpretation. Using the PSF-blurred image in Figure 3(b) as $\mathbf{m}_{mig}$, we solve the image deblurring problem and obtain the reflectivity model as shown in Figure 3(c). In this test, the L_1-norm of $(\mathbf{m}-\mathbf{m}_{mig})$ is used for the 2nd term in Equation 4. Clearly the resolution of Figure 3(c) is much higher than the one of Figure 3(b). Compared to Figure 3(b), the edges of reflectivities are much sharper and more geological structures are exposed for seismic interpretation. It is clear that the reconstructed reflectivities in Figure 3(c) are perceptually similar to the original reflectivities in Figure 3(a).

Using the same acquisition geometry and wavelet as what we used for the calculation of PSFs, we generate synthetic seismic data from the velocity model shown in Figure 1(a). The 2nd synthetic data is migrated with the smoothed velocity model in Figure 1(b). The migration image in the rectangular area in Figure 1(a) is displayed in Figure 4(a). Since the velocity models are different for the modeling and RTM, migration artifacts are observed. This test is similar to most real problems in which subsurface velocities are seldom well known, particularly in geologically complex structures. Since RTM tries to push seismic waves back to their reflecting points, it is essential that the waves be pushed backward through the same

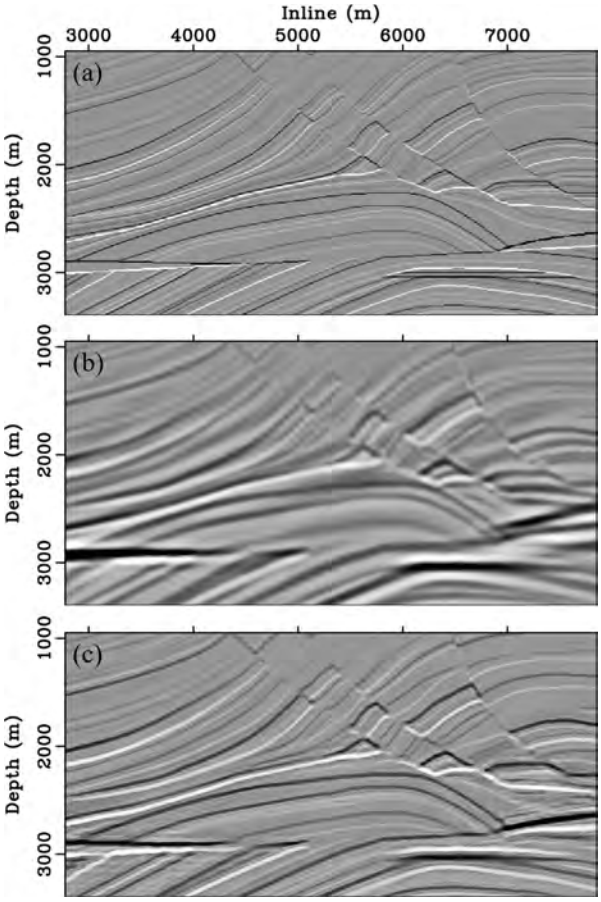

Figure 3: (a) Reflectivities computed from the velocity model given in the rectangular area in Figure 1(a). (b) Image $\mathbf{m}_{mig}$ obtained through the convolution of the reflectivities in 3(a) with the calculated PSFs shown in Figure 2. Theoretically, the image is equivalent to a conventional migration image. (c) Reflectivities calculated from Equation 4 with the L_1-norm of $(\mathbf{m}-\mathbf{m}_{mig})$ of the 2nd term.

medium through which they have propagated. In this case, seismic waves are not able to get back to their correct positions at a given time since the migration velocity used in RTM differs from the actual velocity.

The LSM of the migration image is computed with the 2nd term being the L_2- and L_1-norm of $(\mathbf{m}-\mathbf{m}_{mig})$ in the objective function 4. In order to find optimal reflectivity models, 50 iterations are implemented in the non-linear conjugate gradient method. The obtained reflectivity models are displayed in Figure 4(c) and (e), respectively. As expected, the LSM scheme reduces migration artifacts and significantly improves image resolution in both vertical and horizontal directions and, thus, broadens the spectra in the k_x-k_z domain. The comparison of the results with the 2nd term being the L_2- and L_1-norm of $(\mathbf{m}-\mathbf{m}_{mig})$ indicates that the L_1-norm gives us much sharper and more continuous seismic events in the reflectivity model and a much wider spectrum, especially in the k_z direction, in the wavenumber domain.

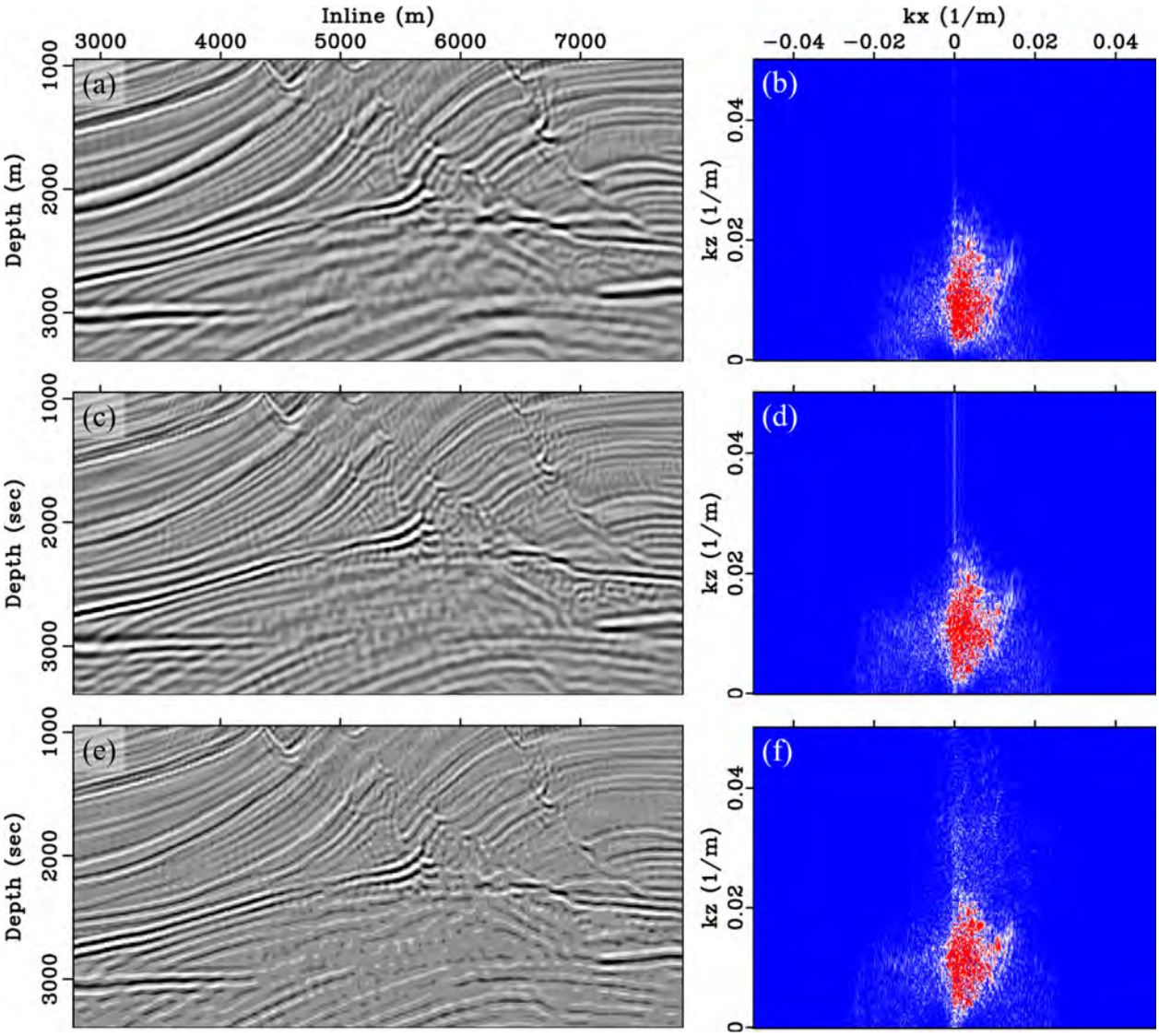

Figure 4: (a) Migration image from RTM. (b) Wavenumber-domain spectrum of panel (a). (c) Reflectivity model obtained from Equation 4 with the L_2-norm of $(\mathbf{m} - \mathbf{m}_{mig})$ of the 2nd term. (d) Wavenumber-domain spectrum of panel (c). (d) Reflectivity model obtained from Equation 4 with the L_1-norm of $(\mathbf{m} - \mathbf{m}_{mig})$ of the 2nd term. (f) Wavenumber-domain spectrum of panel (e). The migration image and reflectivity models are from the rectangular area highlighted in Figure 1(a).

CONCLUSIONS

In this paper we present a multi-iteration image-domain LSM scheme through PSFs with the L_p-norm regularization of the difference between $\mathbf{m}$ and $\mathbf{m}_{mig}$ and the TV regularization of the model $\mathbf{m}$. The L_p-norm regularization is helpful in reducing artifacts and keeping $\mathbf{m}$ similar to $\mathbf{m}_{mig}$, while the TV regularization is introduced to keep the continuity of geological structures. In this LSM scheme we approximate the Hessian through PSFs. The synthetic seismic data for a grid of scatterer points is generated through the linearized Born modeling operators and, then, is migrated through RTM to calculate the PSFs. The same FD kernel is used for the modeling and migration. The tests with the modified Marmousi model shows that the LSM scheme with the L_2- and L_1-norm regularization of $(\mathbf{m}$ - $\mathbf{m}_{mig})$ reduces migration artifacts, significantly improves resolution in migration image and, therefore, broadens amplitude spectra in the wavenumber domain. Although we show the validity of the LSM scheme through RTM, the scheme can be applied to improve migration images produced by other technologies, such as, Kirchhoff migration or one-way wave-equation migration.

ACKNOWLEDGMENTS

We would thank Institut Français du Pétrole for the Marmousi model.

REFERENCES

Aoki, N., and G. T. Schuster, 2009, Fast least-squares migration with a deblurring filter: Geophysics, **74**, no, 6, WCA83–WCA93, doi: https://doi.org/10.1190/1.3155162.

Bai, J., and D. Yingst, 2014, Simultaneous inversion of velocity and density in time-domain full waveform inversion: 84th Annual International Meeting, SEG, Expanded Abstracts, doi: https://doi.org/10.1190/segam2014-0532.1.

Baysal, E., D. D. Kosloff, and J. W. C. Sherwood, 1992, Reverse time migration: Geophysics, **48**, 1514–1524, doi: https://doi.org/10.1190/1.1441434.

Claerbout, J. F., 1985, Imaging the earth's interior: Blackwell Scientific Publications.

Fletcher, R. P., S. Archer, D. Nichols, and W. Mao, 2012, Inversion after depth imaging: 82nd Annual International Meeting, SEG, Expanded Abstracts, doi: https://doi.org/10.1190/segam2012-0427.1.

Golub, G. H., and U. von Matt, 1997, Generalized cross-validation for large-scale problems: Journal of Computational and Graphical Statistics, **6**, 1–34, doi: https://doi.org/10.2307/1390722.

Guitton, A., 2004, Amplitude and kinematic corrections of migrated images for nonunitary imaging operators: Geophysics, **69**, 1017–1024, doi: https://doi.org/10.1190/1.1778244.

Guo, S., and H. Wang, 2020, Image domain least-squares migration with a hessian matrix estimated by non- stationary matching filters: Journal of Geophysics and Engineering, **17**, 148–159, doi: https://doi.org/10.1093/jgehttps://doi.org//gxz098.

Lecomte, I., 2008, Resolution and illumination analyses in PSDM: A ray-based approach: The Leading Edge, **27**, 650–663, doi: https://doi.org/10.1190/1.2919584.

Nemeth, T., C. Wu, and G. T. Schuster, 1999, Least-squares migration of incomplete reflection data: Geophysics, **64**, 208–221, doi: https://doi.org/10.1190/1.1444517.

Ristow, D., and T. Rühl, 1997, 3-d implicit finite-difference migration by multiway splitting: Geophysics, **62**, 554–567, doi: https://doi.org/10.1190/1.1444165.

Wu, D., G. Yao, J. Cao, and Y. Wang, 2016, Least-squares rtm with L_1 norm regularisation: Journal of Geophysics and Engineering, **13**, 666–673, doi: https://doi.org/10.1088/1742-2132/13/5/666.